On the numerical approximation of ∞-harmonic mappings

Nonlinear Differ. Equ. Appl. (2016) 23:61

1021-9722/16/060001-23
published online November 8, 2016
DOI 10.1007/s00030-016-0415-9

Nonlinear Differential Equations and Applications NoDEA

On the numerical approximation of ∞-harmonic mappings

Nikos Katzourakis and Tristan Pryer

Abstract. A map $u : \Omega \subseteq \mathbb{R}^n \longrightarrow \mathbb{R}^N$, is said to be ∞-harmonic if it satisfies

$$\Delta_\infty u := \Big(\mathrm{D}u \otimes \mathrm{D}u + |\mathrm{D}u|^2 [\![\mathrm{D}u]\!]^\perp \otimes I\Big) : \mathrm{D}^2 u = 0. \tag{1}$$

The system (1) is the model of vector-valued Calculus of Variations in L^∞ and arises as the "Euler-Lagrange" equation in relation to the supremal functional

$$E_\infty(u, \Omega) := \|\mathrm{D}u\|_{L^\infty(\Omega)}. \tag{2}$$

In this work we provide numerical approximations of solutions to the Dirichlet problem when $n = 2$ and in the vector valued case of $N = 2, 3$ for certain carefully selected boundary data on the unit square. Our experiments demonstrate interesting and unexpected phenomena occurring in the vector valued case and provide insights on the structure of general solutions and the natural separation to phases they present.

Mathematics Subject Classification. Primary 35J47, 35J62, 53C24; Secondary 49J99.

Keywords. ∞-Laplacian, Vector-valued Calculus of Variations in L^∞, Interfaces, Phase separation.

1. Introduction

Let $n, N \in N$ and Ω an open set in $\mathbb{R}^n$. Given a smooth map $u : \Omega \subseteq \mathbb{R}^n \longrightarrow \mathbb{R}^N$ with components $(u_1, \dots, u_N)^\intercal$, the Jacobian matrix map $\mathrm{D}u : \Omega \longrightarrow \mathbb{R}^{Nn}$ is denoted by $\mathrm{D}u = (\mathrm{D}_i u_\alpha)_{i=1\dots n}^{\alpha=1\dots N}$ and the Hessian tensor $\mathrm{D}^2 u : \Omega \longrightarrow \mathbb{R}_s^{Nn^2}$ is denoted by $\mathrm{D}^2 u = (\mathrm{D}^2_{ij} u_\alpha)_{i,j=1\dots n}^{\alpha=1,\dots N}$. We use $\mathbb{R}^{Nn}$ and $\mathbb{R}_s^{Nn^2}$ to denote respectively the matrix space and the symmetric tensor space in

N.K. was partially supported through the EPSRC Grant EP/N017412/1. T.P. was partially supported through the EPSRC Grant EP/P000835/1.

which $\mathrm{D}u$ and D^2u are valued. In this paper we are interested in the numerical approximation of solutions to the ∞-Laplacian which is defined on smooth maps as the following PDE system

$$\Delta_\infty u \,:=\, \Big(\mathrm{D}u\otimes\mathrm{D}u+|\mathrm{D}u|^2[\![\mathrm{D}u]\!]^\perp\otimes I\Big):\mathrm{D}^2u \,=\, 0 \qquad \text{on } \Omega. \tag{1.1}$$

In the above, "$\otimes$" denotes the algebraic tensor product, "$|\mathrm{D}u|$" denotes the Frobenius norm of the Jacobian in the matrix space $\mathbb{R}^{Nn}$, that is

$$|\mathrm{D}u|^2 \,:=\, \sum_{\alpha=1}^{N}\sum_{i=1}^{n}\mathrm{D}_iu_\alpha\,\mathrm{D}_iu_\alpha\,,$$

"I" is the identity matrix and, given a linear map $A:\mathbb{R}^n\longrightarrow\mathbb{R}^N$, "$[\![A]\!]^\perp$" denotes the orthogonal projector onto the orthogonal complement of the range $R(A)$ of the map:

$$[\![A]\!]^\perp \,:=\, \mathrm{Proj}_{(R(A))^\perp}. \tag{1.2}$$

Note that $R(A)$ and $(R(A))^\perp$ are vector subspaces of $\mathbb{R}^N$. The notation ":" symbolises a contraction with respect to 3 indices as above which extends the Frobenius inner product in $\mathbb{R}^{Nn}$. In index form with respect to the canonical bases, (1.1) reads

$$\sum_{\beta=1}^{N}\sum_{i,j=1}^{n}\Big(\mathrm{D}_iu_\alpha\,\mathrm{D}_ju_\beta\,+\,|\mathrm{D}u|^2[\![\mathrm{D}u]\!]^\perp_{\alpha\beta}\,\delta_{ij}\Big)\mathrm{D}^2_{ij}u_\beta\,=\,0,\qquad \alpha=1,\ldots,N.$$

The system (1.1) (whose solution we call ∞-harmonic mappings) arises as the analogue of the Euler-Lagrange equations associated to the supremal functional

$$E_\infty(u,\Omega)\,:=\,\|\mathrm{D}u\|_{L^\infty(\Omega)}\,. \tag{1.3}$$

The functional (1.3) and the PDE system (1.1) are the archetypal model objects of vector-valued Calculus of Variations in the space L^∞. Throughout this exposition we will use the terminology *scalar* to denote the case $N=1$ and *vectorial* to denote the case $N>1$. In the scalar case, the system (1.1) simplifies to the following single equation

$$\mathrm{D}u\otimes\mathrm{D}u:\mathrm{D}^2u\,=\,\sum_{i,j=1}^{n}\mathrm{D}_iu\,\mathrm{D}_ju\,\mathrm{D}^2_{ij}u\,=\,0 \tag{1.4}$$

since the second term involving the orthogonal projection (1.2) vanishes identically. The field of Calculus of Variations in the space L^∞ was initiated by Aronsson in the 1960s [1–6] where (1.4) was derived and its relation to variational problems arising from (1.3) was explored. Since then, the field has recieved considerable interest within the PDE community [8,12,19, c.f.]. Up to the early 2010s, all considerations were restricted to the scalar case. The general vectorial case of (1.1) as well as the study of the associated PDE systems arising from more general first order functionals

$$E_\infty(u,\Omega) := \left\| H(\cdot,u,\mathrm{D}u) \right\|_{L^\infty(\Omega)} \tag{1.5}$$

has been initiated in a series of recent papers [20–28]. Besides the intrinsic mathematical interest of the field, L^∞ functionals can be applied in a variety of scenarios. A specific example arises in the study of polycrystals, see [10] where the authors use supremal functionals to describe the plasticity of these polycrystals.

A fundamental difficulty arising already in the scalar case is that (1.4) is degenerate elliptic and not in divergence form. This means classical approaches to define and study weak solutions via integration-by-parts fail. In general the Dirichlet problem cannot be solved in the class of smooth functions. Indeed, Aronsson himself demonstrated the existence of singular solutions in [6,7] which are minimisers of the functional. The theory of viscosity solutions of Crandall–Ishii–Lions [12,14,19] proved to be the appropriate framework in which to seek "weak" solutions for scalar L^∞ variational problems.

In the vectorial case, as in the scalar case, solutions of (1.1) may also be singular [20,22] but in addition to this further difficulties arise in the vectorial case that are not present in the scalar case. One such issue is that the projection $[\![\mathrm{D}u]\!]^\perp$ may be discontinuous even for C^∞ maps u, whence the nonlinear operator Δ_∞ of (1.2) may have discontinuous coefficients even when applied to C^∞ maps. This happens because the range of the Jacobian matrix $\mathrm{D}u(x) \in \mathbb{R}^{Nn}$ may not be constant throughout the domain Ω. The appropriate duality-free notion of generalised solution for (1.1) has very recently been proposed in [26] and is based on the probabilistic representation of the Hessian. The latter may not exist classically and we define it "weakly" in a duality-free manner by considering the limits of difference quotients as Young measures. In this setting, existence of a solution to the Dirichlet problem (1.1) and for the more general class of equations arising from (1.5) for $n = 1$ has been proven [27]. Another difficulty is that solutions to (1.1) are not in general unique [24]. This is typical when studying systems of equations, also arising in the area of conservation laws for example, and appropriate *selection criterion* must be employed to pick a "good" solution. For (1.1) we advocate the use of p-approximation, the approximation of ∞-harmonic mapping with p-harmonic ones for increasing p, as a selection criterion and illustrate, at least numerically, that this is reasonable.

In the scalar case some numerical schemes have been proposed for the direct approximation of viscosity solutions of (1.4). In [16,34,35] Oberman uses techniques from Barles and Souganidis [11] for the approximation of fully nonlinear PDEs to construct *wide stencil* difference schemes for the ∞-Laplacian. See also [33] where the authors construct a local mesh refinement (h-adaptive) finite element scheme based on a residual error indicator and the method derived in [32]. Herein we report on numerical experiments that provide further understanding of ∞-harmonic mappings. To the best of our knowledge, the experiments we perform have not been attempted in the vectorial case elsewhere. We consider a set of five different boundary conditions on the unit square $\Omega = (-1,1)^2$ with targets as either $\mathbb{R}^2$ or $\mathbb{R}^3$ (Sects. 4.3–4.6). The

method we follow is based on the approximation of the L^∞ system (1.1) by the respective L^p Euler-Lagrange system, that is the p-Laplacian

$$\Delta_p u := \operatorname{div}\left(|\mathrm{D}u|^{p-2}\mathrm{D}u\right) = 0, \tag{1.6}$$

for large $p \in N$. Our numerical scheme of choice is the finite element method. We utilise the approach described in [36] for the scalar version of (1.1) where it was shown that by forming an appropriate limit we are able to select candidates for numerical approximation along a "good" sequence of solutions, the p-harmonic mappings. This approach has been analytically justified in the scalar case of (1.4) in [36]. Herein we justify its application to the full vectorial case of (1.1).

The numerical method we employ is a finite element approximation, based on an earlier work of Barrett and Liu on numerical methods for elliptic systems [9]. Therein the authors prove that, for a fixed exponent p, the method converges to the respective p-harmonic mapping under certain regularity assumptions on the solution. We would like to stress that significant care must be taken with numerical computations using this approach because the resulting nonlinear system is ill-conditioned. This owes to the nonlinearity of the problem which grows exponentially with p. Work to overcome this issue includes, for example, the work of Huang et al. [17] where preconditioners based on gradient descent algorithms are designed and shown to work well for p up to 1000. We circumvent the need for such preconditioners by choosing our boundary data carefully such that $|\mathrm{D}u| \approx 1$ over the domain allowing us to control the nonlinearity $|\mathrm{D}u|^p$ for large p.

The purpose of this work is to demonstrate some key properties of ∞-harmonic mappings by using an analytically justifiable numerical scheme which currently is the *only* technique available to give insight into the limiting vector-valued problem. We note that our goal is *not* to construct an efficient approximation method for the ∞-Laplace system; indeed this indirect approximation of the ∞-Laplacian system by variational problems is not computationally efficient.

Our results exhibit some interesting phenomena arising as $p \to \infty$. More specifically, as p increases the image of the solutions tends to "flatten" and they behave like minimal surfaces. If the boundary condition includes two components which have ranks equal to $1, 2$ (Sects. 4.3, 4.4), then the solutions tend to achieve the maximum possible rank throughout the domain. Moreover, as p increases the angle between the 2 partial derivative vectors appears to approach a constant value throughout without any interfaces inside the domain. If we prescribe boundary data which have rank equal to 1 (Sect. 4.5), then as p increases the solutions tend to "break" and attain rank 1 for $p = \infty$ without interfaces, while for all finite p there is a region whereon the rank of the gradient is 2 and nontrivial interfaces appear. However, in general interfaces may be formed and they may not be either smooth or with locally Euclidean topology: in Sects. 4.6 and 4.7 we use as boundary data the *explicit* ∞-harmonic maps constructed in [21] whose interfaces are either rectangular or with triple

junctions. Our results show that the p-harmonic maps approach the explicit solutions as p increases, forming interfaces with these shapes.

We conclude this introduction by noting that in the paper [37] the authors derived a different more singular multi-valued version of "∞-Laplacian" which describes optimal Lipschitz extensions. In our setting this amounts to changing in (1.3) from the Euclidean norm "$|\cdot|$" we are using on $\mathbb{R}^{Nn}$ to the nonsmooth operator norm $\|A\| = \max_{|a|=1} |Aa|$.

2. Basics on Vectorial Calculus of Variations in L^∞ and its Fundamental Equations

2.1. L^p approximations as $p \longrightarrow \infty$ of the L^∞ equations

The nomenclature ∞-Laplacian of (1.1) owes to its very derivation as the limit of the p-Laplacian (1.6) as $p \to \infty$. In addition, the respective functionals also approximate the L^∞ functional, if rescaled appropriately, in that for any $W^{1,\infty}(\Omega)$ function we have

$$E_p(u,\Omega) := \left(\int_\Omega |\mathrm{D}u|^p\right)^{1/p} \longrightarrow \|\mathrm{D}u\|_{L^\infty(\Omega)} = E_\infty(u,\Omega), \quad \text{as } p \to \infty. \tag{2.1}$$

In the vectorial case the derivation of the full system (1.1) from (1.6) was first performed in [20]. We recall here the *formal* derivation which is the scaffolding we employ for the numerical approximations to our solutions. Suppose $u : \Omega \longrightarrow \mathbb{R}^N$ is a smooth map. We rewrite the p-Laplacian (1.6) in index form as

$$\sum_{i=1}^n \mathrm{D}_i \left(|\mathrm{D}u|^{p-2}\mathrm{D}_i u_\alpha\right) = 0, \qquad \alpha = 1,\dots,N. \tag{2.2}$$

By distributing derivatives, we have

$$\sum_{\beta=1}^N \sum_{i,j=1}^n (p-2)|\mathrm{D}u|^{p-4}\mathrm{D}_i u_\alpha\, \mathrm{D}_j u_\beta\, \mathrm{D}^2_{ij} u_\beta + |\mathrm{D}u|^{p-2}\sum_{i=1}^n \mathrm{D}^2_{ii} u_\alpha = 0, \qquad \alpha = 1,\dots,N$$

and we may normalise and contract the derivatives in the first summand to find

$$\sum_{i=1}^n \left(\mathrm{D}_i u_\alpha\, \mathrm{D}_i\Big(\frac{1}{2}|\mathrm{D}u|^2\Big) + \frac{|\mathrm{D}u|^2}{p-2}\mathrm{D}^2_{ii} u_\alpha\right) = 0, \qquad \alpha = 1,\dots,N.$$

In vector notation this means

$$\mathrm{D}u\,\mathrm{D}\Big(\frac{1}{2}|\mathrm{D}u|^2\Big) + \frac{|\mathrm{D}u|^2}{p-2}\Delta u = 0. \tag{2.3}$$

If we let $p \to \infty$ in (2.3), we *lose information* and we formally obtain only the system $\mathrm{D}u \otimes \mathrm{D}u : \mathrm{D}^2 u = 0$ which is one of the components of (1.1). In the scalar case this idea is correct and we obtain the full equation (1.4). In the general vectorial case, we have the information that the two summands of (2.3) are opposite and in particular $|\mathrm{D}u|^2\Delta u$ is tangential to the image

$u(\Omega) \subseteq \mathbb{R}^N$. In order to retain this information, for any fixed $x \in \Omega$ we split $\mathbb{R}^N$ as the direct orthogonal sum of the range of $\mathrm{D}u(x) : \mathbb{R}^n \longrightarrow \mathbb{R}^N$ and of its complement

$$\mathbb{R}^N \;=\; R(\mathrm{D}u(x)) \oplus R(\mathrm{D}u(x))^{\perp}$$

and by recalling (1.2), we also set

$$[\![\mathrm{D}u(x)]\!]^{\parallel} \;:=\; \mathrm{Proj}_{R(\mathrm{D}u(x))} \;=\; I \;-\; [\![\mathrm{D}u(x)]\!]^{\perp}. \tag{2.4}$$

By utilising (2.4) and (1.2), we split the system (2.3) as follows

$$\Big\{\mathrm{D}u\,\mathrm{D}\Big(\frac{1}{2}|\mathrm{D}u|^2\Big) \;+\; \frac{|\mathrm{D}u|^2}{p-2}[\![\mathrm{D}u]\!]^{\parallel}\Delta u\Big\} \;+\; \frac{1}{p-2}\Big\{|\mathrm{D}u|^2[\![\mathrm{D}u]\!]^{\perp}\Delta u\Big\} \;=\; 0. \tag{2.5}$$

Note now that for each $x \in \Omega$ the term in the first bracket is valued in $R(\mathrm{D}u(x))$, while the second term is orthogonal to the first and is valued in $R(\mathrm{D}u(x))^{\perp}$. Hence, the two summands are linearly independent. We choose to renormalise (2.5) by multiplying the second summand by $p-2$. Then, after this normalisation we see

$$\mathrm{D}u\,\mathrm{D}\Big(\frac{1}{2}|\mathrm{D}u|^2\Big) \;+\; |\mathrm{D}u|^2[\![\mathrm{D}u]\!]^{\perp}\Delta u \;=\; -\,\frac{|\mathrm{D}u|^2}{p-2}[\![\mathrm{D}u]\!]^{\parallel}\Delta u. \tag{2.6}$$

By letting $p \to \infty$ in (2.6) we obtain the full system (1.1). A byproduct of this derivation is that (1.1) actually can be decoupled to a pair of systems (tangential and normal) which are independent of one another:

$$\mathrm{D}u \otimes \mathrm{D}u : \mathrm{D}^2u \;=\; 0, \qquad |\mathrm{D}u|^2[\![\mathrm{D}u]\!]^{\perp}\Delta u \;=\; 0. \tag{2.7}$$

Although the above arguments, (2.3)–(2.7) do not make sense rigorously for classical C^2 solutions, they are very instructive of the approach we follow. In the scalar case the above method of studying the L^∞ equations by utilising the asymptotic limits of the L^p equations as $p \to \infty$ has proved to be successful. This idea, which dates back to Aronsson, has been effectively put into action by applying the theory of viscosity solutions to the ∞-Laplacian (see e.g. [12,19] and references therein) which, in view of the equivalence of weak and viscosity solutions [18,31] for the p finite case, is very stable under limits. Further, in view of the uniqueness in the scalar case, all subsequential limits as $p \to \infty$ give rise to a viscosity solution of the limit equation.

In the vectorial case the situation is much more complicated since there is no effective counterpart of viscosity solutions stable under limits which would allow for existence proofs with elementary estimates. Motivated partly by the equations arising in L^∞, a duality-free theory of generalised solutions which applies to general fully nonlinear systems of any order [26]. In particular, it allows to make sense of (1.1) in the appropriate regularity class of $W^{1,\infty}(\Omega,\mathbb{R}^N)$ mappings. Among other results, in [26] is the existence of a solution to the Dirichlet problem for (1.1) and in [28] variational characterisations of ∞-harmonic maps in terms of the functional (1.3) are proven. The idea behind this new notion of so-called $\mathcal{D}$-*solutions* is briefly explained in Sects. 2.3.

Due to these additional complications arising in the vectorial case it is impossible to obtain uniqueness for the Dirichlet problem to (1.1) even in the class of C^∞ solutions and for $n = N = 2$ [24]. Evidence provided herein suggests that *the method of L^p approximations as $p \to \infty$ provides a necessary selection principle to pick a "good" solution to* (1.1) *which is conjectured to be unique.*

We now state an existence result for asymptotic limits of p-harmonic maps as $p \to \infty$ needed later. The proof can be found in [36] and is a minor vectorial extension of standard results on limits of p-harmonic functions as $p \to \infty$. Since the proof utilises only arguments involving norms, the proof in the vectorial case is essentially the same as in the scalar case [19,36]. Let us also remind here the standard notion of weak solutions to the p-Laplacian: a map $u \in W^{1,p}_g(\Omega, \mathbb{R}^N)$ is weakly p-harmonic when

$$\int_\Omega |\mathrm{D}u|^{p-2}\,\mathrm{D}u : \mathrm{D}v = \int_\Omega f \cdot v, \quad \forall\, v \in W^{1,p}_0(\Omega, \mathbb{R}^N). \tag{2.8}$$

Theorem 2.2. *(Existence of limits of p-harmonic maps as $p \to \infty$) Let $\{u_p\}_{p=1}^\infty$ denote a sequence of weak solutions to the p-Laplace system* (1.6) *with $u_p \in W^{1,p}_g(\Omega, \mathbb{R}^N)$. Then, there exists a subsequence such that as $p \to \infty$ that sequence converges uniformly to a mapping $u_\infty \in W^{1,\infty}(\Omega, \mathbb{R}^N)$. Namely,*

$$u_{p_j} \longrightarrow u_\infty \text{ in } C^0(\overline{\Omega}, \mathbb{R}^N), \quad \text{as } p \to \infty. \tag{2.9}$$

We emphasise that the map u_∞ is a *candidate* ∞-harmonic mapping, that is a generalised solution to (1.1). This is true in the scalar case $N = 1$ in the sense of viscosity solutions of Crandall–Ishii–Lions [14,36]. In the vectorial case when $n = 1$, it is true in the sense of $\mathcal{D}$-solutions of [27]. We conjecture this to also be true in the case of (1.1) when both $n, N > 1$, but this is not a consequence of the current results of [26] since the method of the existence proof was based on an ad-hoc method (an analytic counterpart of Gromov's "Convex Integration" for a differential inclusion) rather than on p-harmonic approximations. A complete proof of this conjecture, at least to date, eludes us, but recently we have made significant progress in this regard.

2.3. Generalised solutions of the L^∞ equations

For the sake of completeness we briefly motivate here the definition of generalised solutions to (1.1). Since we do not utilise it in an essential manner in this paper, we refrain from giving all the details which can be found in [26] and [27–30]. The idea applies to general fully nonlinear systems of any order and allows for merely measurable solutions. It is based on the following observation: a map $u : \Omega \longrightarrow \mathbb{R}^N$ in $C^2(\Omega, \mathbb{R}^N)$ is a solution to (1.1) if and only if for any compactly supported function $\Phi \in C^0_c(\mathbb{R}^{Nn^2}_s)$, we have

$$\int_{\mathbb{R}^{Nn^2}_s} \Phi(\mathscr{X}) \left(\mathrm{D}u \otimes \mathrm{D}u + |\mathrm{D}u|^2[\mathrm{D}u]^\perp \otimes I\right) : \mathscr{X}\, d[\delta_{\mathrm{D}^2 u}](\mathscr{X}) = 0, \quad \text{on } \Omega. \tag{2.10}$$

The equation (2.10) is a mere restatement of the system (1.1) where we just change the viewpoint and instead of considering the Hessian as a classical map $\mathrm{D}^2 u : \Omega \longrightarrow \mathbb{R}^{Nn^2}_s$, we instead view it as a probability valued map given by the Dirac mass at the Hessian:

$$x \longmapsto \delta_{\mathrm{D}^2 u(x)} \ : \ \Omega \longrightarrow \mathscr{P}(\mathbb{R}^{Nn^2}_s).$$

Note that by attaching one point and compactifying $\mathbb{R}^{Nn^2}_s$ for any map there always exist limits of the difference quotients in the appropriate space of probability-valued maps. These may not be the concentration measures $\delta_{\mathrm{D}^2 u}$ but instead more general probability valued maps $\mathcal{D}^2 u : \Omega \longrightarrow \mathscr{P}(\mathbb{R}^{Nn^2}_s \cup \{\infty\})$ called *diffuse Hessians*. More precisely, if $D^{1,h}$ denotes the first difference quotient operator on $\mathbb{R}^n$, our generalised Hessians are the subsequential limits of the form

$$\delta_{D^{1,h}\mathrm{D}u} \overset{*}{\rightharpoonup} \mathcal{D}^2 u, \quad \text{as } h \to 0 \text{ in the Young measures } \ \Omega \longrightarrow \mathbb{R}^{Nn^2}_s \cup \{\infty\}.$$

The respective generalisation of (2.10) is called a $\mathcal{D}$*-solution* to the ∞-Laplacian (1.1) and is the primary notion of generalised solution in this context for the vectorial case.

2.4. Some explicit smooth ∞-harmonic mapping in 2×2 dimensions

The following explicit solutions of the system (1.1) have been constructed in [21] and we briefly recall them here because they are utilised later in Sect. 3. Let $u : \mathbb{R}^2 \longrightarrow \mathbb{R}^2$ be a map in $C^1(\mathbb{R}^2, \mathbb{R}^2)$. We set

$$\begin{cases} \Omega_2 := \Big\{ x \in \mathbb{R}^2 \ : \ \mathrm{rank}\big(\mathrm{D}u(x)\big) = 2 \Big\}, \\ \Omega_1 := \mathrm{int}\Big\{ x \in \mathbb{R}^2 \ : \ \mathrm{rank}\big(\mathrm{D}u(x)\big) \leq 1 \Big\}, \\ \mathcal{S} \ := \mathbb{R}^2 \setminus (\Omega_1 \cup \Omega_2). \end{cases} \tag{2.11}$$

Here "int" denotes the topological interior. We call Ω_2 *the* 2*-dimensional phase,* Ω_1 *the* 1*-dimensional phase and* $\mathcal{S}$ *the interface* of the map u and notice that $\mathbb{R}^2 = \Omega_2 \cup \Omega_1 \cup \mathcal{S}$. On Ω_2 u is a local diffeomorphism and on Ω_1 it is "essentially scalar". In [21] we proved that the explicit formula

$$u(x, y) \ := \ \int_y^x e^{i\kappa(t)} \, \mathrm{d}t \tag{2.12}$$

defines a smooth explicit ∞-harmonic map $(-1, 1)^2 \subseteq \mathbb{R}^2 \longrightarrow \mathbb{R}^2$ when $\kappa \in C^1(\mathbb{R})$ and $\|\kappa\|_{C^0(\mathbb{R})} < \pi/2$. Here, recall that we are using e^{it} to symbolise $(\cos(t), \sin(t))^{\intercal}$. Moreover:

(I) If κ is qualitatively as in Fig. 1a, namely $\kappa \equiv 0$ on $(-\infty, 0]$ and $\kappa' > 0$ on $(0, \infty)$, then u is affine on Ω_1 and Ω_1, Ω_2, $\mathcal{S}$ are as in Fig. 1c, i.e.

$$\Omega_1 = \{x, y < 0\}, \quad \mathcal{S} = \boldsymbol{p}\Omega_1 \cup \{x = y \geq 0\}, \quad \Omega_2 = \mathbb{R}^2 \setminus (\Omega_1 \cup \mathcal{S}).$$

(II) If κ is qualitatively as in Fig. 1b, namely if $\kappa \equiv 0$ on $[-1, +1]$ and $\kappa' > 0$ on $(-\infty, -1) \cup (1, \infty)$, then u is affine on Ω_1 and Ω_1, Ω_2, $\mathcal{S}$ are as in Fig. 1d, i.e.

$$\Omega_1 = \{-1 < x, y < 1\}, \quad \mathcal{S} = \boldsymbol{p}\Omega_1 \cup \{x = y, |y| \geq 1\}, \quad \Omega_2 = \mathbb{R}^2 \setminus (\Omega_1 \cup \mathcal{S}).$$

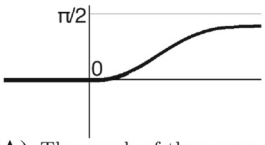

(A) The graph of the parametrisation function κ of (I) used in 2.12.

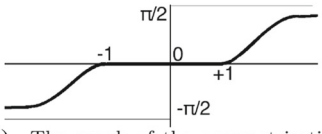

(B) The graph of the parametrisation function κ of (II) used in 2.12.

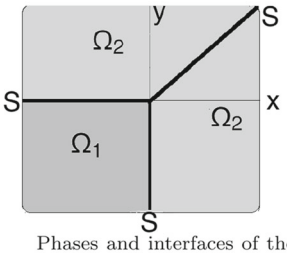

(C) Phases and interfaces of the smooth ∞-harmonic map given by the explicit formula 2.12 when κ is as in (I).

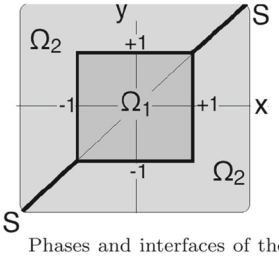

(D) Phases and interfaces of the smooth ∞-harmonic map given by the explicit formula 2.12 when κ is as in (II).

FIGURE 1. Illustrations of explicit solutions to the ∞-Laplace system with $n = N = 2$

These examples show that in the vectorial case very complicated phenomena can arise even for smooth solutions. We will further examine these phenomena in Sect. 4 numerically by studying p-harmonic mappings for increasing values of p using boundary data provided by (2.12) with choices of κ as in (I) and (II).

3. Numerical Approximations of ∞-harmonic mappings for $n = N = 2$ and $n = 2 < N = 3$

In this Section we describe the technique we use to approximate ∞-harmonic mappings. The method we use is a conforming finite element discretisation of the p-Laplacian analysed in [9] for fixed p. We will describe the discretisation and justify its application to the problem at hand by studying the behaviour as the meshsize parameter tends to zero and as p gets large. To that end we will also extend the results given in [36] to the vectorial case.

We let $\mathscr{T}$ be an admissible triangulation of Ω, namely, $\mathscr{T}$ is a finite collection of sets such that

(1) $K \in \mathscr{T}$ implies K is an open triangle,
(2) for any $K, J \in \mathscr{T}$ we have that $\overline{K} \cap \overline{J}$ is either $\emptyset$, a vertex, an edge, or the whole of $\overline{K}$ and $\overline{J}$ and
(3) $\bigcup_{K\in\mathscr{T}} \overline{K} = \overline{\Omega}$.

The shape regularity constant of $\mathscr{T}$ is defined as the number

$$\mu(\mathscr{T}) := \inf_{K\in\mathscr{T}} \frac{\rho_K}{h_K}, \tag{3.1}$$

where ρ_K is the radius of the largest ball contained inside K and h_K is the diameter of K. An indexed family of triangulations $\{\mathscr{T}^n\}_n$ is called *shape regular* if

$$\mu := \inf_n \mu(\mathscr{T}^n) > 0. \tag{3.2}$$

Further, we define the piecewise constant *meshsize function* of $\mathscr{T}$ to be

$$h(x) := \max_{K \ni x} h_K. \tag{3.3}$$

A mesh is called quasiuniform when there exists a positive constant C such that $\max_{x\in\Omega} h(x) \leq C \min_{x\in\Omega} h(x)$. In what follows we shall assume that all triangulations are shape regular and quasiuniform. Further, whenever we write h without argument, we consistently refer to $h = \max_{K\in\mathscr{T}} h_K$.

We let $\mathbb{P}^k(\mathscr{T})$ denote the space of piecewise polynomials of degree k over the triangulation $\mathscr{T}$, i.e.,

$$\mathbb{P}^k(\mathscr{T}) = \left\{\phi \text{ such that } \phi|_K \in \mathbb{P}^k(K)\right\} \tag{3.4}$$

and introduce the *finite element space*

$$\mathbb{V} := \mathbb{P}^k(\mathscr{T}) \cap \mathrm{C}^0(\Omega) \tag{3.5}$$

as the space of continuous piecewise polynomial functions of at most degree k.

Definition 3.1. *($L^2(\Omega)$ projection operator) The $L^2(\Omega)$ projection operator, $P_h : L^2(\Omega) \longrightarrow \mathbb{V}$ is defined for $w \in L^2(\Omega)$ such that*

$$\int_\Omega P_h w\, v_h = \int_\Omega w\, v_h, \quad \forall\, v_h \in \mathbb{V}. \tag{3.6}$$

It is well known that this operator satisfies the following approximation properties for $w \in W^{1,p}(\Omega)$ [13]

$$\lim_{h\to 0} \|w - P_h w\|_{L^p(\Omega)} = 0 \tag{3.7}$$

$$\lim_{h\to 0} \|\mathrm{D}w - \mathrm{D}(P_h w)\|_{L^p(\Omega)} = 0. \tag{3.8}$$

We consider the Galerkin discretisation of (2.2), to find $u_{h,p} \in \mathbb{V}^N$ with $u_{h,p}|_{\partial\Omega} = P_h g$ such that

$$\int_\Omega |\mathrm{D}u_{h,p}|^{p-2}\, \mathrm{D}u_{h,p} : \mathrm{D}v_h = 0, \qquad \forall\, v_h \in \mathbb{V}^N. \tag{3.9}$$

This is a conforming finite element discretisation of the vectorial p-Laplacian system proposed in [9].

Proposition 3.2. *(existence and uniqueness of solution to (3.9)) There exists a unique solution of both the weak formulation (2.8) and the Galerkin approximation (3.9).*

Proof. Existence and uniqueness of this problem follows from examination of the p-functional

$$E_p(u,\Omega) = \left(\int_\Omega |\mathrm{D}u|^p\right)^{1/p}. \tag{3.10}$$

Notice that (3.10) is strictly convex and coercive on $W_0^{1,p}(\Omega,\mathbb{R}^N)$ so we may apply standard arguments from the Calculus of Variations showing that the minimisation problem is well posed. Hence, there exists $u \in W_g^{1,p}(\Omega,\mathbb{R}^N)$ such that

$$E_p(u,\Omega) = \min_{v\in W_0^{1,p}(\Omega,\mathbb{R}^N)} E_p(v,\Omega). \tag{3.11}$$

Noticing that the weak problem (2.8) is the weak Euler-Lagrange equation for (3.11) we have equivalence of (2.8) and (3.11) as such the weak formulation is also well posed. To see this for the Galerkin approximation notice that $\mathbb{V}^N \subset W^{1,p}(\Omega,\mathbb{R}^N)$. As such the minimisation problem over $\mathbb{V}^N$ is equivalent to (3.9) and the same argument applies as in the continuous case. □

Theorem 3.3. *(convergence of the discrete scheme to weak solutions) For fixed p let $(u_{h,p})_h$ be the finite element approximation generated by solving (3.9) and u_p, the weak solution of (2.8), then we have that*

$$u_{h,p} \longrightarrow u_p \quad \text{in } \mathrm{C}^0(\overline{\Omega},\mathbb{R}^N), \text{ as } h \to 0. \tag{3.12}$$

Proof. We begin by noting the discrete weak formulation (3.9) is equivalent to the minimisation problem: Find $u_{h,p} \in \mathbb{V}^N$ with $u_{h,p}|_{\partial\Omega} = P_h g$ such that

$$E_p(u_{h,p},\Omega) = \min_{v_h\in\mathbb{V}^N} E_p(v_h,\Omega). \tag{3.13}$$

Using this, we immediately have

$$\|\mathrm{D}u_{h,p}\|^p_{L^p(\Omega)} \le E_p(u_{h,p},\Omega) \le E_p(P_h g,\Omega) \le \|\mathrm{D}(P_h g)\|^p_{L^p(\Omega)}. \tag{3.14}$$

In view of the stability of the L^2 projection in $W^{1,p}(\Omega)$ [15] we have

$$\|\mathrm{D}u_{h,p}\|_{L^p(\Omega)} \le C, \tag{3.15}$$

uniformly in h. Hence by weak compactness there exists a (weak) limit to the finite element sequence, which we will call u^*. Due to the weak semicontinuity of $E_p(\cdot,\Omega)$ we have

$$E_p(u^*,\Omega) \le E_p(u_{h,p},\Omega). \tag{3.16}$$

In addition, in view of the approximation properties of P_h given in Definition 3.1 we have for any $v \in \mathrm{C}^\infty(\Omega,\mathbb{R}^N)$ that

$$E_p(v,\Omega) = \liminf_{h\to 0} E_p(P_k v,\Omega). \tag{3.17}$$

Using the fact that $u_{h,p}$ is a discrete minimiser of (3.13) we have

$$E_p(u^*,\Omega) \le E_p(u_{h,p},\Omega) \le E_p(P_h v,\Omega), \tag{3.18}$$

whence sending $h \longrightarrow 0$ we see

$$E_p(u^*,\Omega) \le E_p(v,\Omega). \tag{3.19}$$

Now, as v was generic we may use density arguments and that u_p was the unique minimser to conclude $u^* = u_p$, concluding the proof. □

Theorem 3.4. *(convergence) Let $u_{h,p}$ be the Galerkin solution of (3.9) and u_∞ the candidate ∞-harmonic mapping. Then, along a subsequence we have*

$$u_{h,p_j} \longrightarrow u_\infty \text{ in } \mathrm{C}^0, \text{ as } p \to \infty \text{ and } h \to 0. \tag{3.20}$$

Proof. The proof consists of combining Theorems 2.2 and 3.3 and noticing that

$$\left\|u_{h,p_j} - u_\infty\right\|_{\mathrm{C}^0(\Omega)} \leq \left\|u_{h,p_j} - u_{p_j}\right\|_{\mathrm{C}^0(\Omega)} + \left\|u_{p_j} - u_\infty\right\|_{\mathrm{C}^0(\Omega)}, \tag{3.21}$$

as required. □

Remark 3.5. (*convergence up to a subsequence*) The result of Theorem 3.4 shows convergence of the p-approximation, and indeed the Galerkin approximation, up to a subsequence. As already mentioned, in the vectorial problem there is *no unique solution* to this problem, hence different subsequences could tend to different limits. We conjecture that the p-approximation procedure is a good *selection criteria* for this problem. In the next section we will numerically demonstrate this, although analytically we are, at the time of the writing of this article, unable to show this.

4. Numerical experiments

In this Section we summarise extensive numerical experiments which focus on quantifying the structure of solutions to the ∞-Laplacian PDE system (1.1). This is achieved using Galerkin approximations to the p-Laplacian for sufficiently high values of p. We focus on studying the behaviour solutions have as p increases which allow us to make various conjectures on the behaviour of their asymptotic limit as $p \to \infty$.

Remark 4.1. (*practical computation of (3.9) for large p*) The computation of p-harmonic mappings is an extremely challenging problem in its own right. The class of nonlinearity in the problem results in the algebraic system, which ultimately yields the finite element solution, being ill-conditioned. One method to tackle this class of problems is by using preconditioners based on descent algorithms [17]. For extremely large p, say $p \geq 10000$, this may be required; however for our purposes we restrict our attention to $p \sim 1000$. This yields sufficient accuracy for the results we want to illustrate.

We emphasise that even the case $p \sim 1000$ is computationally tough to handle. The numerical approximation we are using is based on a damped Newton solver. Such methods require a good initial guess in order to achieve converge. A reasonable initial guess for the p-Laplacian is given by numerically approximating with the q-Laplacian for $q < p$ sufficiently close to p. This leads to an iterative process in the generation of the initial guess, i.e., we solve the 2-Laplacian as an initial guess to the 3-Laplacian which serves as an initial guess to the 4-Laplacian, and so on. In each of our experiments the number of Newton iterations required to achieve a relative tolerance of 10^{-8} was achieved in less that 20 iterations.

Remark 4.2. (*rates of convergence of the scheme*) Using the methodology of p-approximation which we advocate here it has been numerically demonstrated in the scalar case the rates of convergence both in p and in h that we expect to achieve [36, Section 4]. It was noticed that these rates were dependant on the regularity of the underlying ∞-harmonic function and that

$$\|u_\infty - u_{h,p^*}\|_{L^\infty} \approx \mathrm{O}(h) \tag{4.1}$$

for solutions $u_\infty \in \mathrm{C}^\infty$ and

$$\|u_\infty - u_{h,p^*}\|_{L^\infty} = \mathrm{O}(h^{1/3}) \tag{4.2}$$

if $u_\infty \in \mathrm{C}^{1,1/3}$. Where we use p^* as the smallest p such that $\inf_p \|u_\infty - u_{h,p}\|_{L^\infty}$ is achieved.

In both cases as h is decreased, an increasing value of p is required to achieve optimal approximation (in h). This suggests a coupling $p = Ch^\alpha$ is necessary to achieve convergence, where the α is determined by the regularity expected in u_∞. We found experimentally that coupling $p = h^{-1/2}$ worked well for the singular case ($u_\infty \in \mathrm{C}^{1,1/3}$) and $p = h^{-1}$ for the smooth case ($u_\infty \in \mathrm{C}^\infty$).

In the vectorial case, which is the focus of this work, we observed the same convergence phenomena with the smooth solutions we test in Sects. 4.6 and 4.7.

We mention that we do *not* have access to exact solutions in general. For the experiments in Sects. 4.3–4.5 we only provide boundary data and in principle the solutions to this problem are non-smooth and must be interpreted in the $\mathcal{D}$-sense described in Sect. 2.

To tie into the explicit examples given in Fig. 1 we are particularly interested in the rank of the solution. Except for the intrinsic interest, this relates directly to a deeper understanding of the solutions to ∞-Laplace system since the coefficients of (1.1) are discontinuous on the interfaces of the solution. We compute this by calculating $\det(\mathrm{D}u_{h,p})$ and representing the areas Ω_2, Ω_1 and $\mathcal{S}$ of (2.11) by plotting contours of the function $\det(\mathrm{D}u_{h,p})$.

4.3. Solutions $(-1,+1)^2 \longrightarrow \mathbb{R}^2$ with mixed rank-two and rank-one boundary data

In this test we construct approximations of solutions of (1.1) with mixed rank-two and rank-one boundary data. We take

$$g(x,y) := \begin{cases} \frac{1}{2}(x,y)^\intercal, & \text{if } x \geq 0 \text{ or } y \leq 0, \\ \frac{1}{4}(x+y-1, x+y+1)^\intercal, & \text{otherwise.} \end{cases} \tag{4.3}$$

This gives us rank-one data in the quadrant $x < 0$ and $y < 0$ and rank-two data elsewhere. The results are illustrated in Fig. 2.

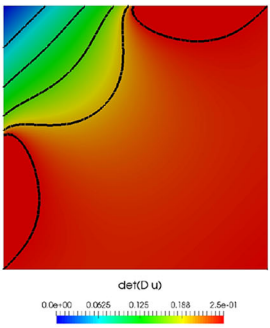

(A) $\det\left(\mathrm{D}u_{h,p}\right)$ for the vectorial 2-Laplacian.

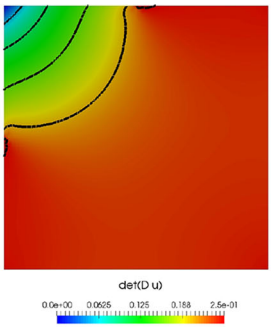

(B) $\det\left(\mathrm{D}u_{h,p}\right)$ for the vectorial 8-Laplacian.

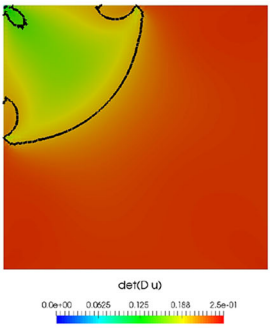

(C) $\det\left(\mathrm{D}u_{h,p}\right)$ for the vectorial 64-Laplacian.

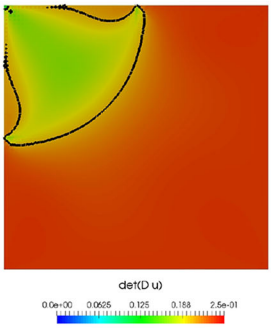

(D) $\det\left(\mathrm{D}u_{h,p}\right)$ for the vectorial 256-Laplacian.

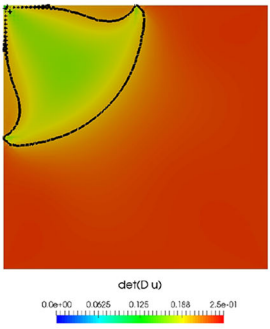

(E) $\det\left(\mathrm{D}u_{h,p}\right)$ for the vectorial 512-Laplacian.

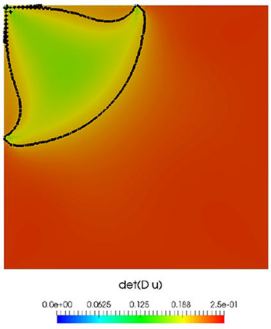

(F) $\det\left(\mathrm{D}u_{h,p}\right)$ for the vectorial 1024-Laplacian.

FIGURE 2. An illustration of the rank of the solution to the vectorial p-Laplacian with the mixed rank-one and rank-two boundary conditions given in Sect. 4.3 for various increasing values of p. Here we plot $\det(\mathrm{D}u_{h,p})$ and associated *contour lines*. These are plotted at increments of 0.05. Notice as p increases, the region where the solution is not of full rank, Ω_1, decreases in size

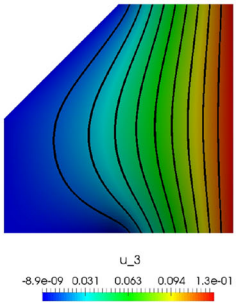

(A) The image of the vectorial 2-Laplacian.

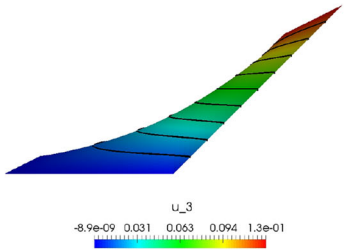

(B) The image of the vectorial 2-Laplacian, side view.

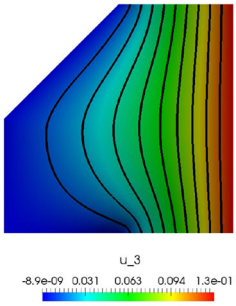

(C) The image of the vectorial 820-Laplacian.

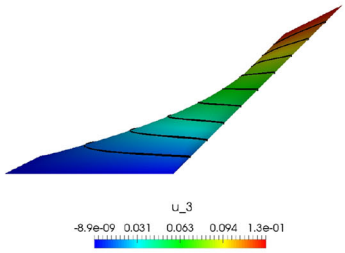

(D) The image of the vectorial 820-Laplacian.

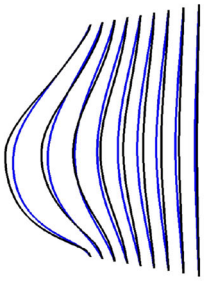

(E) A comparison of the contours. The 2-Laplacian is the lighter colour (blue).

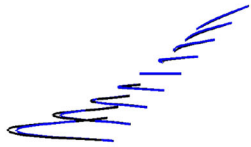

(F) A comparison of the contours from the side view. The 2-Laplacian is the lighter colour (blue).

FIGURE 3. The image of the solution to the vectorial ($N = 3$) p-Laplacian with mixed rank-one and rank-two boundary conditions given in Sect. 4.4 for two values of p.

4.4. Solutions $(-1,+1)^2 \longrightarrow \mathbb{R}^3$ with mixed rank-two and rank-one boundary data

In this experiment we examine an extension to the example given in Sect. 4.3 to the case $N = 3$. We study the image of the problem with boundary data given as

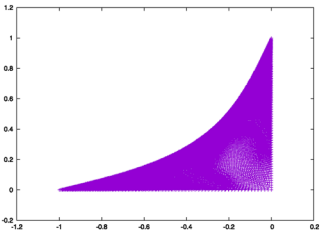

(A) The image of the vectorial 2-Laplacian.

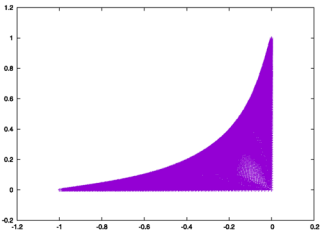

(B) The image of the vectorial 8-Laplacian.

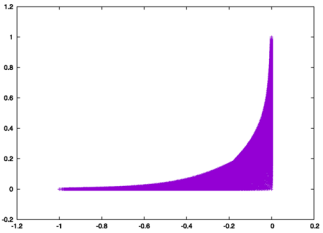

(C) The image of the vectorial 64-Laplacian.

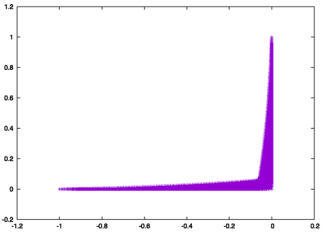

(D) The image of the vectorial 256-Laplacian.

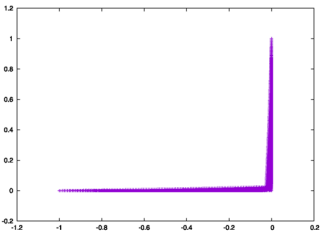

(E) The image of the vectorial 512-Laplacian.

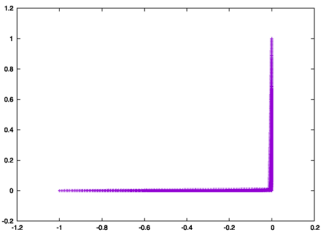

(F) The image of the vectorial 1024-Laplacian.

FIGURE 4. The image of the solution to the vectorial p-Laplacian with the rank-one boundary conditions given in (4.5) for various increasing values of p. Notice as p increases, the image flattens. It is behaving like a minimal surface

$$g(x,y) := \begin{cases} \frac{1}{2}(x,y,x)^{\intercal}, & \text{if } x \geq 0 \text{ or } y \leq 0, \\ \frac{1}{4}(x+y-1, x+y+1, x+y-1)^{\intercal}, & \text{otherwise.} \end{cases} \tag{4.4}$$

4.5. Solutions $(-1,+1)^2 \longrightarrow \mathbb{R}^2$ with rank-one boundary data

In this test we construct mappings with rank-one boundary data. We take

$$g(x,y) := \begin{cases} \boldsymbol{e}_x x, & \text{if} \quad x < 0, \\ \boldsymbol{e}_y x, & \text{if} \quad x \geq 0, \end{cases} \tag{4.5}$$

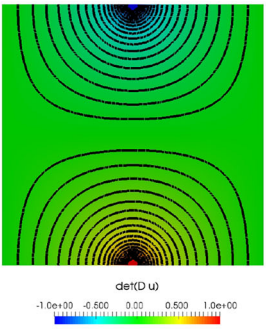

(A) $\det\left(\mathrm{D}u_{h,p}\right)$ for the vectorial 2-Laplacian.

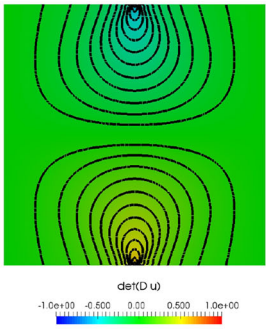

(B) $\det\left(\mathrm{D}u_{h,p}\right)$ for the vectorial 8-Laplacian.

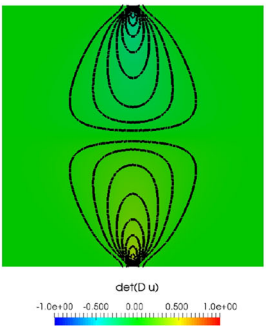

(C) $\det\left(\mathrm{D}u_{h,p}\right)$ for the vectorial 64-Laplacian.

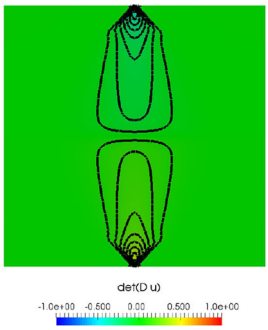

(D) $\det\left(\mathrm{D}u_{h,p}\right)$ for the vectorial 256-Laplacian.

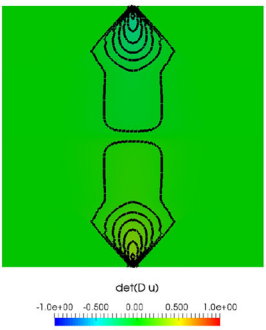

(E) $\det\left(\mathrm{D}u_{h,p}\right)$ for the vectorial 512-Laplacian.

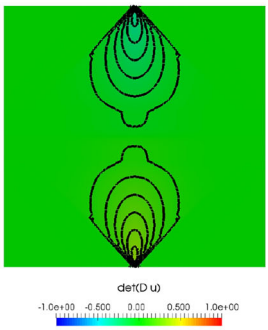

(F) $\det\left(\mathrm{D}u_{h,p}\right)$ for the vectorial 1024-Laplacian.

FIGURE 5. An illustration of the rank of the solution to the vectorial p-Laplacian with the rank-one boundary conditions given in (4.5) for various increasing values of p. Here we plot $\det(\mathrm{D}u_{h,p})$ and associated contour lines. These are plotted at increments of 0.05. Notice as p increases, the solution has lower rank over a larger portion of the domain, that is the size of Ω_1 increases

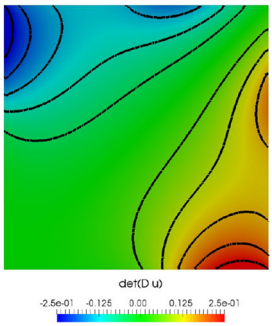

(A) $\det\left(\mathrm{D}u_{h,p}\right)$ for the vectorial 2-Laplacian.

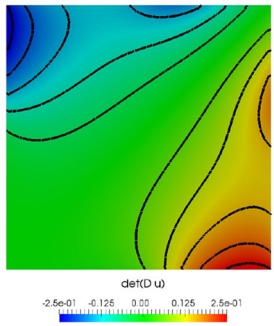

(B) $\det\left(\mathrm{D}u_{h,p}\right)$ for the vectorial 8-Laplacian.

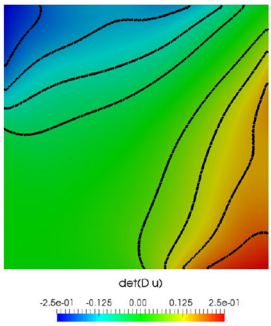

(C) $\det\left(\mathrm{D}u_{h,p}\right)$ for the vectorial 64-Laplacian.

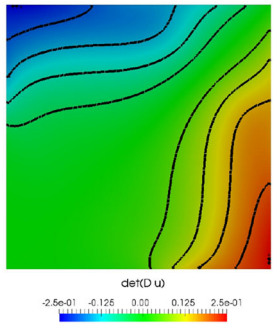

(D) $\det\left(\mathrm{D}u_{h,p}\right)$ for the vectorial 256-Laplacian.

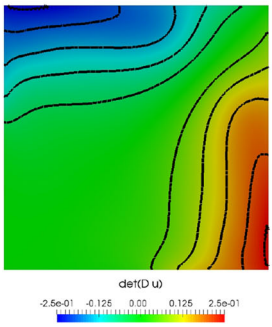

(E) $\det\left(\mathrm{D}u_{h,p}\right)$ for the vectorial 512-Laplacian.

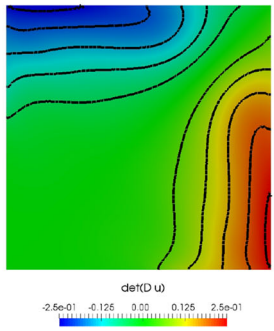

(F) $\det\left(\mathrm{D}u_{h,p}\right)$ for the vectorial 1024-Laplacian.

FIGURE 6. An illustration of the rank of the solution to the vectorial p-Laplacian with the rank-one boundary conditions given in (4.5) for various increasing values of p. Here we plot $\det(\mathrm{D}u_{h,p})$ and associated contour lines. These are plotted at increments of 0.05. Notice as p increases, the structure illustrated in Fig. 1c becomes more pronounced

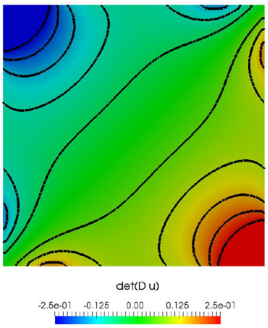

(A) $\det\left(\mathrm{D}u_{h,p}\right)$ for the vectorial 2-Laplacian.

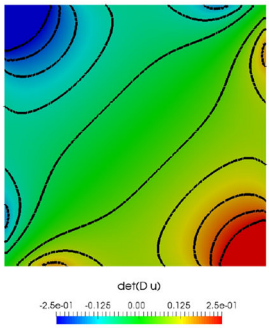

(B) $\det\left(\mathrm{D}u_{h,p}\right)$ for the vectorial 8-Laplacian.

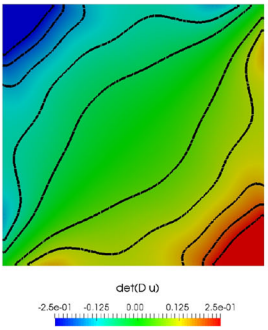

(C) $\det\left(\mathrm{D}u_{h,p}\right)$ for the vectorial 64-Laplacian.

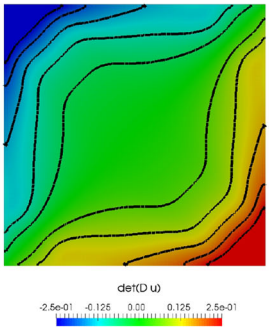

(D) $\det\left(\mathrm{D}u_{h,p}\right)$ for the vectorial 256-Laplacian.

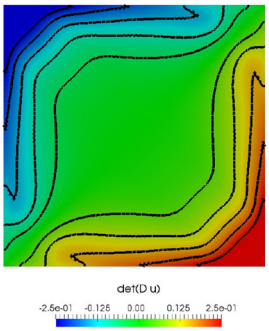

(E) $\det\left(\mathrm{D}u_{h,p}\right)$ for the vectorial 512-Laplacian.

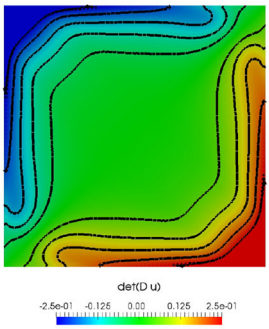

(F) $\det\left(\mathrm{D}u_{h,p}\right)$ for the vectorial 1024-Laplacian.

FIGURE 7. An illustration of the rank of the solution to the vectorial p-Laplacian with the boundary conditions given in 2.12 for the rectangular interface illustrated in Fig. 1c for various increasing values of p. Here we plot $\det(\mathrm{D}u_{h,p})$ and associated contour lines. These are plotted at increments of 0.05. Notice as p increases, the structure illustrated in Fig. 1d becomes more pronounced

where $\boldsymbol{e}_x = (1,0)^{\Vert}$ and $\boldsymbol{e}_y = (0,1)^{\Vert}$ denote the unit vectors in the x and y directions. Notice that $g \in \mathrm{C}^0(\partial\Omega, \mathbb{R}^2)$. We examine the image and rank of the numerical approximation for various values of p in Figs. 4 and 5.

4.6. Solutions $(-1,+1)^2 \longrightarrow \mathbb{R}^2$ with boundary data an explicit ∞-harmonic map with triple junction interface

In this test we construct boundary data which give rise to the example of an explicit smooth ∞-harmonic mapping with a triple junction interface as illustrated in Fig. 1c. We take

$$\kappa(t) := \begin{cases} 1 - \dfrac{1}{1+t^2}, & \text{if} \quad t > 0, \\ 0, & \text{otherwise.} \end{cases} \tag{4.6}$$

We also take

$$g(x,y) := \frac{3}{4}\left(\int_y^x \cos\left(\kappa(t)\right) \mathrm{d}t, \int_y^x \sin\left(\kappa(t)\right) \mathrm{d}t\right)^{\mathsf{T}}. \tag{4.7}$$

The numerical experiment is given in Fig. 6.

4.7. Solutions $(-1,+1)^2 \longrightarrow \mathbb{R}^2$ with boundary data an explicit ∞-harmonic map with rectangular interface

In this test we construct boundary data which give rise to the example of an explicit smooth ∞-harmonic mapping with a box interface as illustrated in Fig. 1d. We take

$$\kappa(t) := \begin{cases} 1 - \dfrac{1}{1+(t-1)^2+1}, & \text{if } t > 1, \\ \dfrac{1}{1+(t+1)^2+1} - 1, & \text{if } t < -1, \\ 0, & \text{otherwise.} \end{cases} \tag{4.8}$$

and

$$g(x,y) := \frac{3}{4}\left(\int_y^x \cos\left(\kappa(t)\right) \mathrm{d}t, \int_y^x \sin\left(\kappa(t)\right) \mathrm{d}t\right)^{\mathsf{T}}. \tag{4.9}$$

The numerical experiment is given in Fig. 7.

References

[1] Aronsson, G.: Minimization problems for the functional $sup_x F(x, f(x), f'(x))$. Arkiv für Mat. **6**, 33–53 (1965)

[2] Aronsson, G.: Minimization problems for the functional $sup_x F(x, f(x), f'(x))$ II. Arkiv für Mat. **6**, 409–431 (1966)

[3] Aronsson, G.: Extension of functions satisfying Lipschitz conditions. Arkiv für Mat. **6**, 551–561 (1967)

[4] Aronsson, G.: On the partial differential equation $u_x^2 u_{xx} + 2u_x u_y u_{xy} + u_y^2 u_{yy} = 0$. Arkiv für Mat. **7**, 395–425 (1968)

[5] G. Aronsson, Minimization problems for the functional $sup_x F(x, f(x), f'(x))$ *III*, Arkiv für Mat. **7**, 509–512 (1969)

[6] Aronsson, G.: On certain singular solutions of the partial differential equation $u_x^2 u_{xx} + 2u_x u_y u_{xy} + u_y^2 u_{yy} = 0$. Manuscr. Math. **47**(1–3), 133–151 (1984)

[7] Aronsson, G.: Construction of singular solutions to the p-harmonic equation and its limit equation for $p = \infty$. Manuscr. Math. **56**, 135–158 (1986)

[8] Barron, N.: Viscosity Solutions and Analysis in L^∞, Nonlinear analysis, differential equations and control (Monttreal QC, 1998), pp. 1–60. Kluwer Academic Publishers, Dordrecht (1998)

[9] Barrett, J.W., Liu, W.B.: Finite element approximation of some degenerate monotone quasilinear elliptic systems. SIAM J. Numer. Anal. **33**(1), 88–106 (1996)

[10] Bocea, M., Nesi, V.: Γ *-convergence of power-law functionals, variational principles in* L_∞ and applications. SIAM J. Math. Anal. **39**(5), 1550–1576. doi:10.1137/060672388

[11] Barles, G., Souganidis, P.E.: Convergence of approximation schemes for fully nonlinear second order equations. Asymptot. Anal. **4**(3), 271–283 (1991)

[12] Crandall, M.G.: A visit with the ∞-Laplacian, in calculus of variations and non-linear PDE, Springer Lecture notes in Mathematics 1927. CIME, Cetraro (2005)

[13] Ciarlet, P.: The finite element method for elliptic problems. North-Holland Publishing Co., Amsterdam (1978) (Studies in Mathematics and its Applications, vol. 4)

[14] Crandall, M.G., Ishii, H., Lions, P.-L.: User's guide to viscosity solutions of 2nd order partial differential equations. Bull. AMS **27**(1), 1–67 (1992)

[15] Crouzeix, M., Thomée, V.: The stability in L_p and W_p^1 of the L_2-projection onto finite element function spaces. Math. Comput. **48**, 521–532 (1987)

[16] Esedoglu, S., Oberman, A.: Fast semi-implicit solvers for the infinity laplace and p-laplace equations. https://arxiv.org/pdf/1107.5278.pdf (2011)

[17] Huang, Y.Q., Li, R., Liu, W.: Preconditioned descent algorithms for p-Laplacian. J. Sci. Comput. **32**, 343–371 (2007)

[18] Juutinen, P., Lindqvist, P., Manfredi, J.: On the equivalence of viscosity solutions and weak solutions for a quasi-linear equation. SIAM J. Math. Anal. **33**(3), 699–717 (electronic) (2001)

[19] Katzourakis, N.: An introduction to viscosity solutions for fully nonlinear PDE with applications to calculus of variations in L^∞. Springer Briefs in Mathematics (2015). doi:10.1007/978-3-319-12829-0

[20] Katzourakis, N.: L^∞-variational problems for maps and the Aronsson PDE system. J. Differ. Equ. **253**(7), 2123–2139 (2012)

[21] Katzourakis, N.: Explicit $2D$ ∞-harmonic maps whose interfaces have junctions and corners. Comptes Rendus Acad. Sci. Paris Ser. I **351**, 677–680 (2013)

[22] Katzourakis, N.: On the structure of ∞-harmonic maps. Commun. PDE **39**(11), 2091–2124 (2014)

[23] Katzourakis, N.: ∞-Minimal submanifolds. Proc. Am. Math. Soc. **142**, 2797–2811 (2014)

[24] Katzourakis, N.: Nonuniqueness in vector-valued calculus of variations in L^∞ and some linear elliptic systems. Commun. Pure Appl. Anal. **14**(1), 313–327 (2015)

[25] Katzourakis, N.: Optimal ∞-quasiconformal immersions. ESAIM Control Opt. Calc. Var. (2015). doi:10.1051/cocv/2014038 (to appear)

[26] Katzourakis, N.: Generalised solutions for fully nonlinear PDE systems and existence-uniqueness theorems. http://arxiv.org/pdf/1501.06164

[27] Katzourakis, N.: Existence of generalised solutions to the equations of vectorial Calculus of Variations in L^∞. http://arxiv.org/pdf/1502.01179

[28] Katzourakis, N.: A new characterisation of ∞-harmonic and p-harmonic mappings via affine variations in L^∞. http://arxiv.org/pdf/1509.01811

[29] Katzourakis, N.: Equivalence between weak and $\mathcal{D}$-solutions for symmetric hyperbolic PDE systems. http://arxiv.org/pdf/1507.03042

[30] Katzourakis, N.: Mollification of $\mathcal{D}$-solutions to fully nonlinear PDE systems. http://arxiv.org/pdf/1508.05519

[31] Katzourakis, N.: Nonsmooth convex functionals and feeble viscosity solutions of singular Euler–Lagrange equations. Calc. Var. Partial Differ. Equ. **54**, 275–298 (2015)

[32] Lakkis, O., Pryer, T.: A finite element method for nonlinear elliptic problems. SIAM J. Sci. Comput. **35**(4), A2025–A2045 (2013)

[33] Lakkis, O., Pryer, T.: An adaptive finite element method for the infinity laplacian. Numer. Math. Advan. Appl. 283–291 (2013)

[34] Oberman, A.: A convergent difference scheme for the infinity Laplacian: construction of absolutely minimizing Lipschitz extensions. Math. Comp. **74**(251), 1217–1230 (electronic) (2005)

[35] Oberman, A.: Finite difference methods for the infinity Laplace and p-Laplace equations. J. Comput. Appl. Math. **254**, 65–80 (2013)

[36] Pryer, T.: On the finite element approximation of Infinity-Harmonic functions. Royal Society of Edinburgh Proceedings (to appear). http://arxiv.org/pdf/1511.00471

[37] Sheffield, S., Smart, C.K.: Vector valued optimal Lipschitz extensions. Commun. Pure Appl. Math. **65**(1), 128–154 (2012)

Nikos Katzourakis and Tristan Pryer
Department of Mathematics and Statistics
University of Reading
Whiteknights
PO Box 220 Reading RG6 6AX
UK
e-mail: t.pryer@reading.ac.uk

Nikos Katzourakis
e-mail: n.katzourakis@reading.ac.uk

Received: 5 November 2015.
Accepted: 13 October 2016.